Electronic Supplementary Information (ESI) for

Photoelectrochemical sandwich immunoassay of CYFRA21-1 based on In_2O_3/WO_3 type-II heterojunction and CdS quantum dots-polydopamine nanospheres labeling

Luyao Liu, Chenglong Sun, Jialin Liu, Yun Du, Qingji Xie*

Key Laboratory of Chemical Biology & Traditional Chinese Medicine Research (Ministry of Education of China), College of Chemistry and Chemical Engineering, Hunan Normal University, Changsha 410081, China

E-mail address: xieqj@hunnu.edu.cn (Q.J. Xie)

Contents

Reagents and instruments

FTO conductive glass was commercially obtained from Zhuhai Kaivo Optoelectronic Technology Co., Ltd. Sodium tungstate ($Na_2WO_4 \cdot 2H_2O$), indium nitrate ($In(NO_3)_3 \cdot 4.5H_2O$), cadmium chloride ($CdCl_2 \cdot 2.5H_2O$), citric acid, CS, sodium sulfide ($Na_2S \cdot 9H_2O$), ascorbic acid (AA), hydrochloric acid (HCl) and ammonia water ($NH_3 \cdot H_2O$) were commercially obtained from the National Chemical Reagents Company of China. Thioglycolic acid (TGA), N-hydroxysuccinimide (NHS), 1-ethyl-3-(3-dimethylaminopropyl) carbodiimide (EDC), dopamine hydrochloride (DA), BSA and GLD were supplied from Sigma-Aldrich. CYFRA21-1 and CYFRA21-1 antibody (Ab) were purchased from Shanghai Linc-Bio Science Co., Ltd. Human immunoglobulin G (IgG), human interleukin-6 (IL-6), procalcitonin (PCT) and cardiac troponin I (cTnI) were purchased from Beijing Bioss Co., Ltd. All other chemicals are of analytical grade or higher quality. The detection and washing buffers used for the immunoassay were 0.1 M phosphate buffered solution (PBS, pH 7.4, 0.1 M KH_2PO_4-K_2HPO_4) and 0.01 M PBS (pH 7.4), respectively. All solutions in the experiments were prepared with Milli-Q ultrapure water (Millipore, ≥ 18 MΩ cm). Normal human serum samples were kindly donated by Hunan Normal University Hospital.

The PEC experiments were performed on a CHI660E electrochemical workstation (Shanghai Chenhua Instrument Co., Ltd.) equipped with a xenon lamp (300-1000 nm wavelength range and 100 mW cm^{-2} optical power density). Cyclic voltammetry (CV), electrochemical impedance spectroscopy (EIS) and Mott-Schottky barrier experiments were conducted on a CHI660E electrochemical workstation using a three-electrode system, with FTO or its modified electrode as the working electrode (effective surface area 0.25 cm^2), a KCl-saturated calomel electrode (SCE) as the reference electrode, and a platinum disk

electrode (3 mm in diameter) as the counter electrode. The potentials are reported versus SCE, except otherwise specified. Scanning electron microscopy (SEM) characterizations were performed on a FEI Helios NanoLab 600i scanning electron microscope equipped with an Oxford energy dispersive X-ray spectroscopy (EDX) detector for elemental analysis. A TECNAI F-30 transmission electron microscopy (TEM) instrument was used for morphology characterization. An Ultima IV X-ray diffraction (XRD) instrument was used for crystal analysis. X-ray photoelectron spectroscopy (XPS) was recorded on a Thermo Scientific K-Alpha instrument. UV-vis diffuse reflectance spectra (DRS, with $BaSO_4$ as a reference) and ultraviolet-visible (UV-vis) absorption spectra were obtained on a UV-2600i UV-vis spectrophotometer. Fourier transform infrared (FT-IR) spectrum was collected on a IRTracer 100 FT-IR spectrophotometer (KBr pellet method). CS film-thickness was evaluated on an Accrion/Nanofilm EP4SE ellipsometer.

Synthesis of polydopamine nanospheres (PDA NSs) and CdS QDs

The self-polymerization of dopamine was carried out in a water/ethanol/ammonia mixed solution to synthesize PDA NSs with a size of ca. 160 nm.[1] Briefly, 2 mL $NH_3 \cdot H_2O$, 40 mL ethanol and 90 mL ultrapure water were mixed with gentle stirring for 30 min at 30 °C. 0.5 g dopamine hydrochloride was dissolved in 10 mL ultrapure water, which was then quickly injected into the above water/ethanol/ammonia mixture. The color of the dispersion immediately turned light yellow and finally dark brown. After continuous stirring for 24 h, the precipitate was collected by centrifugation and washed three times with ultrapure water.

TGA-modified CdS QDs were synthesized according to the reported method.[2] 250 μL TGA was added to a three-necked flask containing 50 mL 10 mM aqueous $CdCl_2$ under nitrogen atmosphere and solution-stirring condition, and the solution pH was adjusted to pH 11 with 1.0 M NaOH, followed by adding 5 mL 0.1 M aqueous Na_2S. After nitrogen treatment for 4 h, the CdS QDs were deposited with acetone and redispersed in ultrapure water to prepare a 1 mg mL^{-1} CdS QDs dispersion. The CdS QDs dispersion was stored in a 4 °C refrigerator away from light.

Quantitative verification of the presence of In_2O_3 and WO_3 on the In_2O_3/WO_3/FTO electrode from the element atomic percentage data in Fig. 1D

FTO conductive glass consists of SiO_2 substrate and F-doped SnO_2. In the EDX of the In_2O_3/WO_3/FTO electrode shown in Fig. 1D, the atomic percentages are 14.01% for Sn element and 10.51% for Si element, and thus the calculated total atomic percentage of O element in SnO_2 and SiO_2 should be 14.01%×2 + 10.51%×2 = 49.04%. The total atomic percentage of oxygen element is 66.68% in Fig. 1D. After deducting the calculated total atomic percentage of O element in SnO_2 and SiO_2 (49.04%), the atomic percentage of the remaining O element, which should logically be equivalent to the total atomic percentage of O element in In_2O_3 and WO_3, is $x_{O(-)}$ = 66.68% - 49.04% = 17.64%.

In Fig. 1D, the atomic percentages are 2.60% for In element and 3.95% for W element, thus the calculated total atomic percentage of O element in In_2O_3 and WO_3 should be $x_{O(In,W)}$ = 2.60%×3/2 - 3.95%×3 = 15.75%.

Considering the complexity of the actual experimental factors (such as the interference of possible trace impurities), the above calculated $x_{O(-)}$ and $x_{O(In,W)}$ agree well with each other, indicating that WO_3 and In_2O_3 indeed coexist on the In_2O_3/WO_3/FTO electrode.

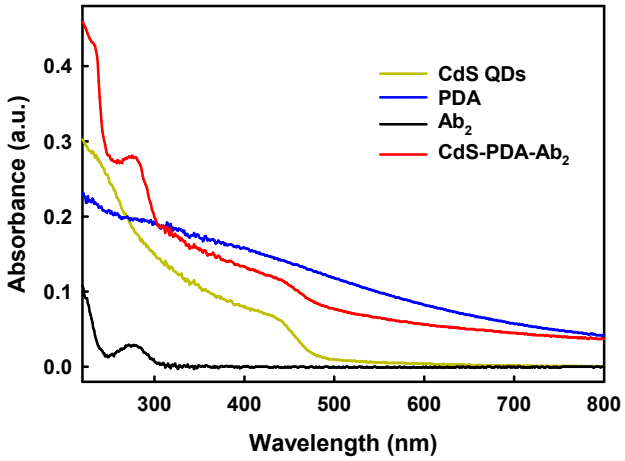

Fig. S1 UV-vis absorption spectra of CdS QDs, PDA, Ab_2 and CdS-PDA-Ab_2.

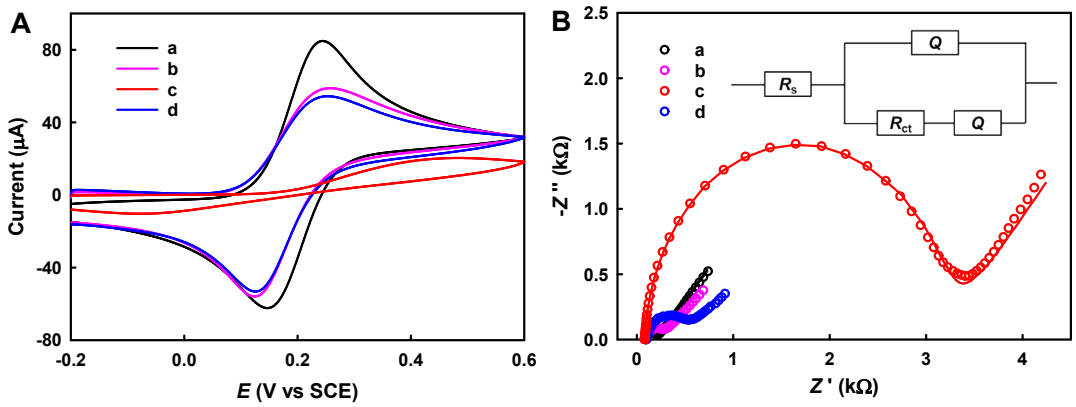

Fig. S2 CV (A, 50 mV s^{-1} scan rate) and EIS (B) curves of FTO (a), In_2O_3/FTO (b), WO_3/FTO (c) and In_2O_3/WO_3/FTO (d) electrodes. Both CV and EIS were performed in 0.01 M PBS (pH 7.4) containing 2.0 mM $K_4[Fe(CN)_6]$ and 0.1 M Na_2SO_4. EIS experiment: 100 kHz~0.01 Hz, 0.20 V bias (the formal potential of $[Fe(CN)_6]^{3-/4-}$ redox couple), 200 s quiet time (to ensure a concentration ratio of 1:1 ($[Fe(CN)_6]^{3-}$ versus $[Fe(CN)_6]^{4-}$) near the electrode surface). Circles: experimental, curves: fitted to the Randles equivalent circuit (inset). The CV oxidation peak current values of the electrodes are ordered as FTO (84.6 μA) > In_2O_3/FTO (59.0 μA) > In_2O_3/WO_3/FTO (54.4 μA) > WO_3/FTO (20.6 μA).

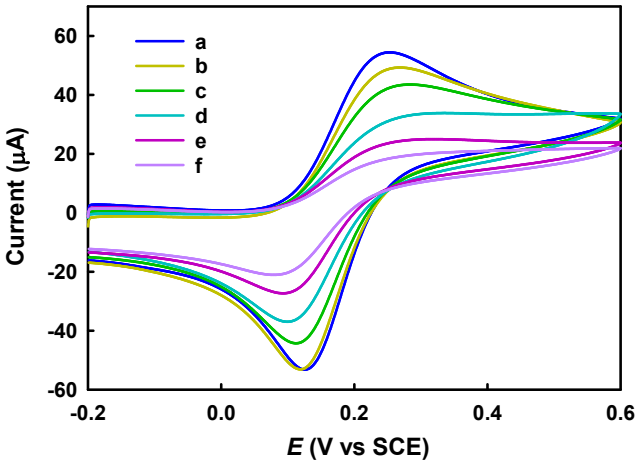

Fig. S3 CV curves on In_2O_3/WO_3/FTO (a), GLD/CS/In_2O_3/WO_3/FTO (b), Ab_1/GLD/CS/In_2O_3/WO_3/FTO (c), BSA/Ab_1/GLD/CS/In_2O_3/WO_3/FTO (d), Ag/BSA/Ab_1/GLD/CS/In_2O_3/WO_3/FTO (e) and BSA/CdS-PDA-Ab_2/Ag/BSA/Ab_1/GLD/CS/In_2O_3/WO_3/FTO (f) electrodes in 0.01 M PBS (pH 7.4) containing 2.0 mM $K_4[Fe(CN)_6]$ and 0.1 M Na_2SO_4. Scan rate: 50 mV s^{-1}. The CV oxidation peak current values are ordered as In_2O_3/WO_3/FTO (54.4 μA) > GLD/CS/In_2O_3/WO_3/FTO (48.8 μA) > Ab_1/GLD/CS/In_2O_3/WO_3/FTO (43.2 μA) > BSA/Ab_1/GLD/CS/In_2O_3/WO_3/FTO (33.9 μA) > Ag/BSA/Ab_1/GLD/CS/In_2O_3/WO_3/FTO (25.2 μA) > BSA/CdS-PDA-Ab_2/Ag/BSA/Ab_1/GLD/CS/In_2O_3/WO_3/FTO (19.7 μA).

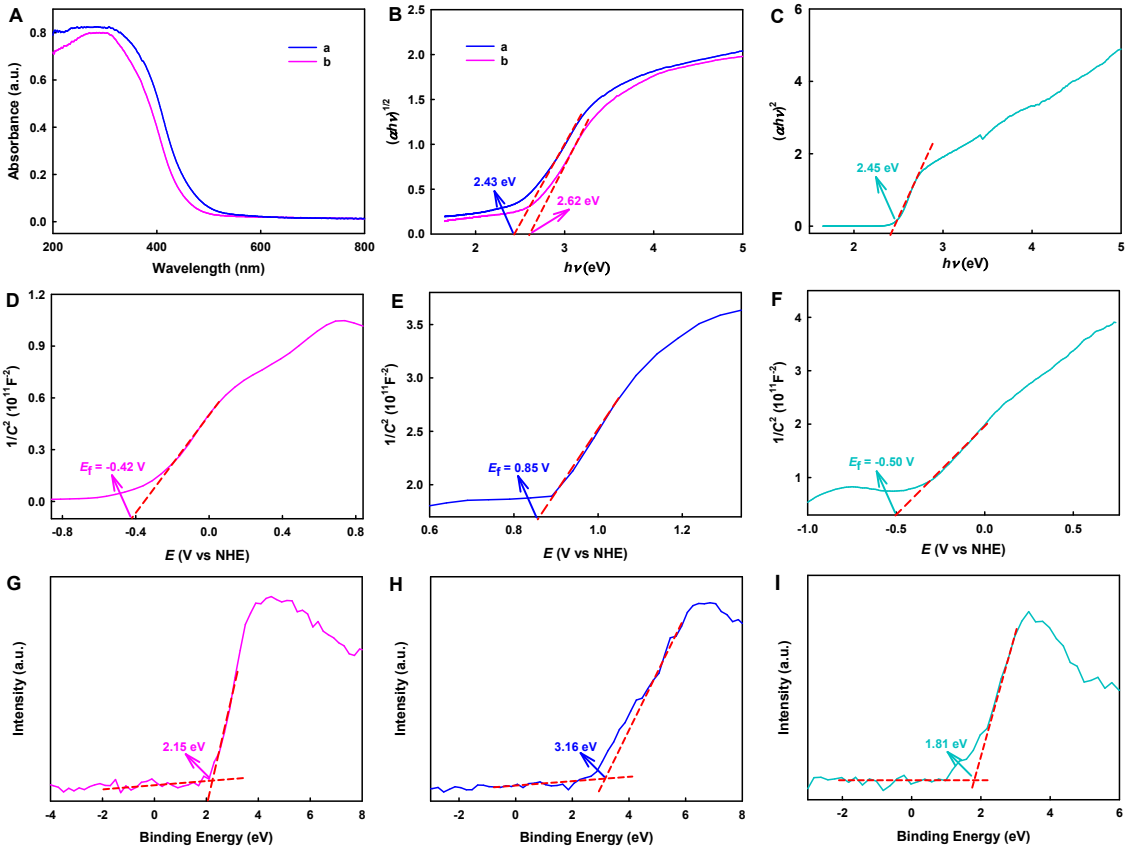

Fig. S4 UV-vis diffuse reflectance spectra (A) and Tauc plots (B) of WO_3 (a) and In_2O_3 (b). Tauc plot of CdS QDs (C). Mott-Schottky plots of In_2O_3 (D), WO_3 (E) and CdS QDs (F). XPS-VB images of In_2O_3 (G), WO_3 (H) and CdS QDs (I). Mott-Schottky experiments: 1000 Hz frequency, 0.2 M aqueous Na_2SO_4.

Here, the forbidden band widths (E_g) of In_2O_3, WO_3 and CdS QDs can be calculated according to the Tauc equation, $\alpha h\nu = A\ (h\nu - E_g)^{m/2}$, where α is the absorption coefficient or the absorbance, ν in s^{-1} is the incident photon frequency, E_g in eV is the band gap, h is Planck's constant (6.63×10^{-34} J s), A is a constant, and m is a variable determined by the transition characteristics of the semiconductor (m=1 for a direct semiconductor and m = 4 for an indirect semiconductor).[3] As shown in Fig. S4B and C, the E_g values of In_2O_3 and WO_3 as indirect semiconductors is obtained as 2.62 eV and 2.43 eV from the plot of $(\alpha h\nu)^{1/2}$ versus $h\nu$, respectively, and the E_g of CdS QDs as a direct semiconductor is obtained as 2.45 eV

according to the plot of $(\alpha hv)^2$ versus hv.[4, 5]

Taking In_2O_3 as an example, we give the calculation details for the band structures. First, the E_g of In_2O_3 is calculated from the UV-vis DRS of In_2O_3 and the Tauc equation. As shown by curve b in Fig. S4A, In_2O_3 has corresponding absorbance values at wavelengths from 200 to 800 nm. The frequency (v) corresponding to a wavelength from 200 nm to 800 nm is equal to the speed of light (ca. 3×10^8 m s^{-1}) divided by the wavelength. Since In_2O_3 is an indirect semiconductor, m is 4. In the Tauc equation, A is a constant whose value has no effect on the calculation result. Therefore, the absorbance value (α value), v value, h (6.63×10^{-34} J s) and m (= 4) obtained at each wavelength can be substituted into the Tauc equation to obtain the Tauc plot of In_2O_3 (Fig. S4B). For example, we obtain α = 0.400 and $v = 7.50\times10^{14}$ s^{-1} at 400 nm, thus $hv = (6.63\times10^{-34}$ J s) $\times$ $(7.5\times10^{14}$ $s^{-1}) = 4.97\times10^{-19}$ J = 3.11 eV (x-axis), and $(\alpha hv)^{1/2}$ = $(0.400 \times 3.11$ eV$)^{1/2} = 1.12$ (y-axis) in Fig. 4B. E_g can be obtained by making the intersection of the tangent and the abscissa. Second, according to the literature,[6, 7] the E_{VB} of In_2O_3 can be obtained by combining the XPS-VB method and linear extrapolation, as shown in Fig. S4G. Finally, substituting the E_g value of 2.62 eV and the E_{VB} value of 2.15 eV into the equation $E_g = E_{VB} - E_{CB}$ gives E_{CB} = 2.15 eV - 2.62 eV = -0.47 eV. The calculations of the band structures of WO_3 and CdS QDs are similar to those of In_2O_3.

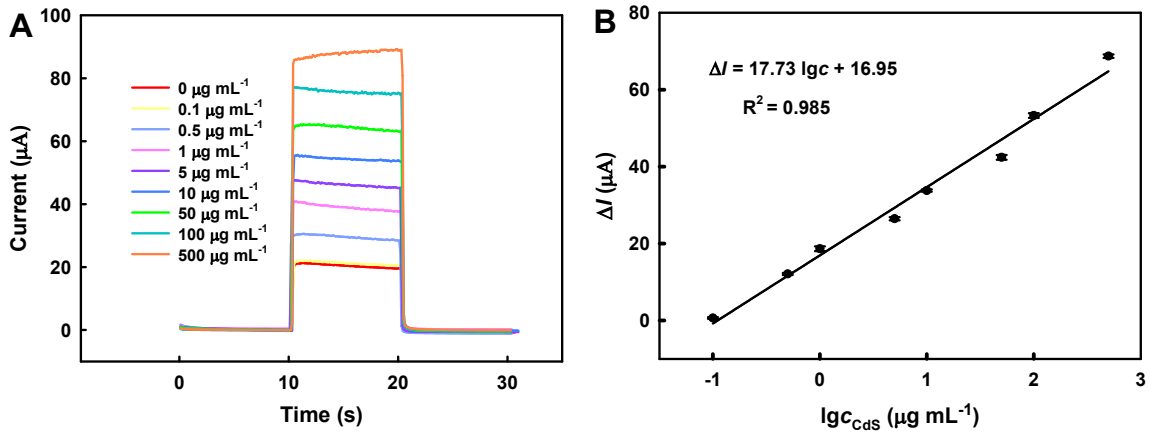

Fig. S5 (A) Photocurrent responses on In_2O_3/WO_3/FTO electrode after cast-coating 20 μL CdS QDs at different concentrations. (B) Corresponding calibration curve. Light on and off at a 10-s interval, -0.05 V bias, 0.1 M PBS (pH 7.4) containing 0.05 M AA.

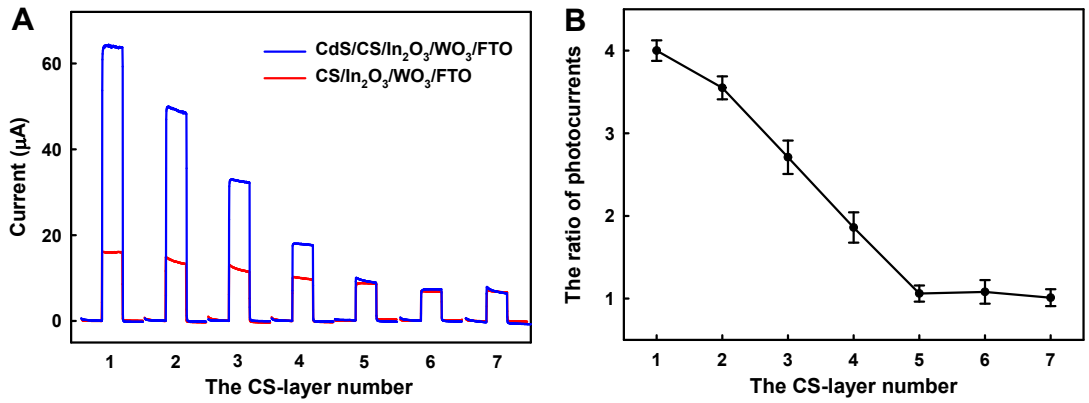

Fig. S6 Photocurrent of dried CdS/CS/In_2O_3/WO_3/FTO and dried CS/In_2O_3/WO_3/FTO electrodes versus number of CS layers (A). Photocurrent ratio of dried CdS/CS/In_2O_3/WO_3/FTO to dried CS/In_2O_3/WO_3/FTO versus number of CS layers (B). Cast-coating 6 μL of 1% acetic acid containing 0.05% CS and/or 20 μL of 0.5 mg mL^{-1} CdS QDs for each modification, -0.05 V bias, 0.1 M PBS (pH 7.4) containing 0.05 M AA.

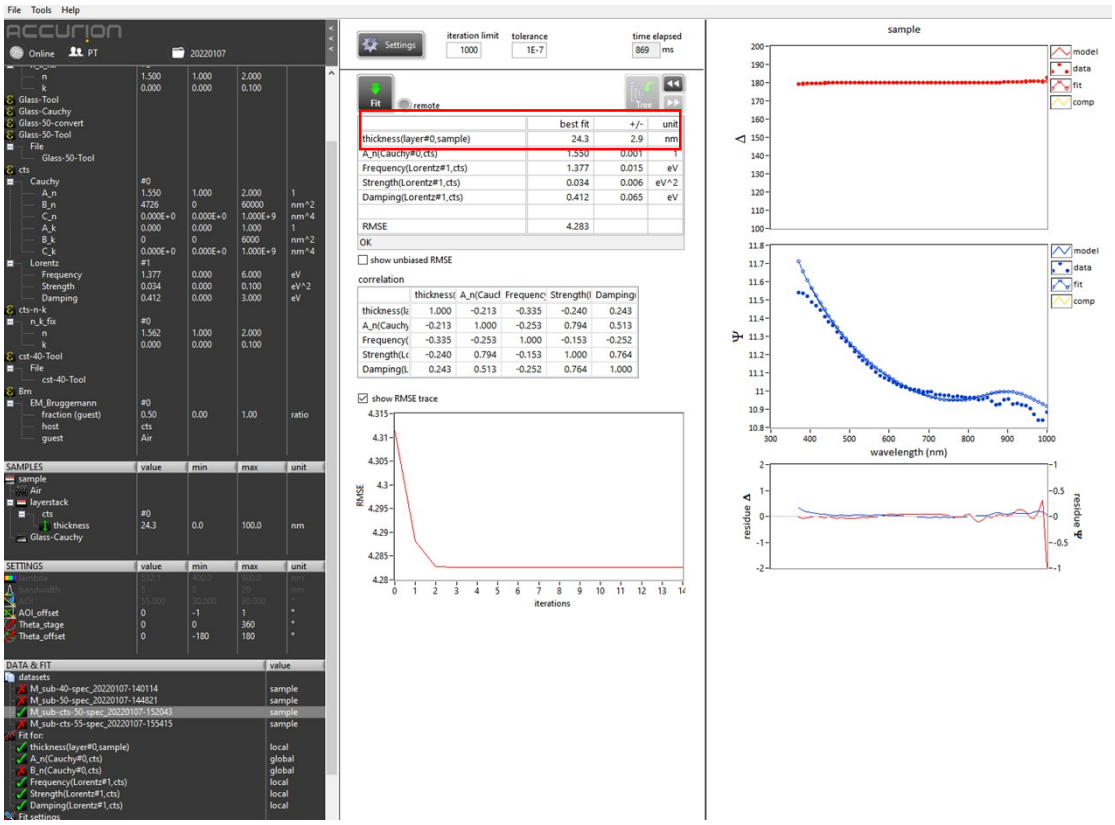

Fig. S7 Nonlinear fitting of the ellipsometric data to obtain the thickness of a single-layer CS film.

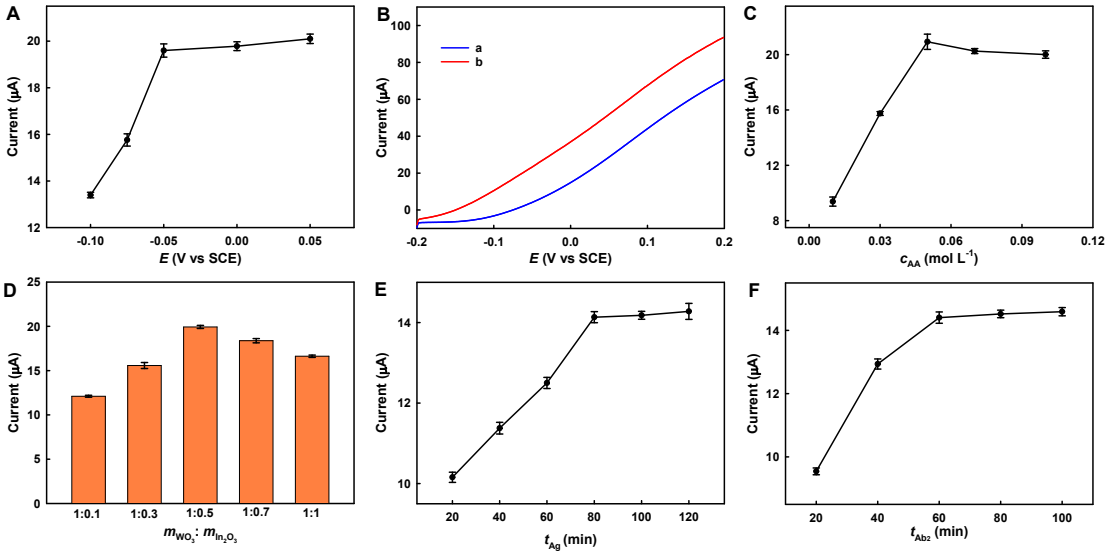

Fig. S8 Optimization of bias potential (A). LSV curves (B, 50 mV s^{-1}) on In_2O_3/WO_3/FTO electrode under light off (a) or light on (b) condition. Optimization of AA concentration (C). Photocurrent response of In_2O_3 and WO_3 versus WO_3-In_2O_3 mass ratio (D). Optimization of 100 pg mL^{-1} Ag incubation time (E) and BSA/CdS-PDA-Ab_2 incubation time (F). Solution: 0.1 M PBS (pH 7.4) containing AA. Bias = -0.05 V, AA concentration (c_{AA}) = 0.05 M, WO_3-In_2O_3 mass ratio (m_{WO3}:m_{In2O3}) = 1:0.5, CYFRA21-1 incubation time (t_{Ag}) = 80 min, and BSA/CdS-PDA-Ab_2 incubation time (t_{Ab2}) = 60 min, except for the parameter under optimization.

As shown in Fig. S8A, the photocurrent of the In_2O_3/WO_3/FTO electrode increases with the positive shift of the bias from -0.1 V to -0.05 V, but the photocurrent is almost stable with the further positive shift of the bias to 0.05 V. Fig. S8B shows the LSV curves of In_2O_3/WO_3/FTO electrode under the condition of switching on or off the lamp. When the potential is greater than -0.05 V, the dark background current generated solely by the electrolysis becomes larger and larger, resulting in the decrease of signal-to-background ratio. Therefore, a bias of -0.05 V (vs SCE) is selected for PEC measurements. In Fig. S8C, the

photocurrent increases when the concentration of ascorbic acid (c_{AA}) is changed from 0.01 M to 0.05 M, and the photocurrent is almost unchanged with the further increase of c_{AA}, indicating that 0.05 M AA is sufficient to clear the holes of In_2O_3/WO_3/FTO. Therefore, 0.05 M AA is selected as the optimal holes scavenger concentration. As shown in Fig. S8D, the maximum photocurrent can be obtained when the mass ratio of WO_3 to In_2O_3 (m_{WO3}:m_{In2O3}) is 1:0.5, probably because other ratios have more electron-hole recombination centers. Furthermore, optimizing the incubation time of Ag and BSA/CdS-PDA-Ab_2 (t_{Ag} and t_{Ab2}) is beneficial to improving the accuracy of the sensor and the experimental efficiency. In Fig. S8E, the photocurrent increases with the increase of t_{Ag}, and the photocurrent is almost unchanged when t_{Ag} is greater than 80 min, indicating that 80 min is sufficient for the specific Ag-Ab_1 immuno-recognition. As shown in Fig. S8F, the photocurrent also increases with the increase of t_{Ab2}, and the photocurrent appears stable after 60 min. Therefore, 80 min and 60 min are selected as the optimal incubation time for Ag and BSA/CdS-PDA-Ab_2, respectively.

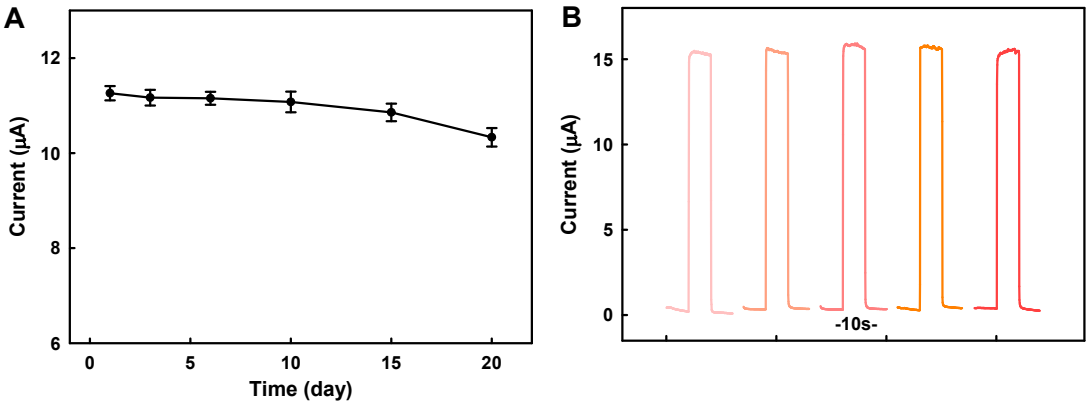

Fig. S9 Long-term stability of PEC immuno-electrode after storage at 4 °C in a refrigerator (A, 1 pg mL^{-1} Ag). Reproducibility of five PEC immuno-electrodes fabricated in batch (B, 500 pg mL^{-1} Ag). -0.05 V bias, 0.1 M PBS (pH 7.4) with 0.05 M AA.

Table S1 Performance comparison for the analysis of CYFRA21-1

Technique	Linear range (ng mL^{-1})	LOD (pg mL^{-1})	Ref.
Lateral flow immunoassay	1.3 ~ 480	160	[8]
Electrochemiluminescence	0.001 ~ 350	0.3	[9]
Electrochemistry	0.0005 ~ 50	0.39	[10]
Electrochemistry	0.25 ~ 800	100	[11]
Electrochemistry	0.01 − 50	10	[12]
Electrochemistry	0 ~ 12	240	[13]
Electrochemistry	0.000625 ~ 0.01	0.625	[14]
PEC	0.0005 ~ 50	0.16	[15]
PEC	0.0001~ 4	0.03	[16]
PEC	0.01 ~ 100	2.5	[17]
PEC	0.0001 ~ 50	0.056	This work

References (The numbering here is valid solely for the ESI)

1. X. X. Guan, X. X. Deng, J. Song, X. Y. Wang and S. Wu, *Anal. Chem.*, 2021, **93**, 6763-6769.
2. F. Xu, Y. C. Zhu, Z. Y. Ma, W. W. Zhao, J. J. Xu and H. Y. Chen, *Chem. Commun.*, 2016, **52**, 3034-3037.
3. Z. T. Yuan, H. S. Huang, N. J. Li, D. Y. Chen, Q. F. Xu, H. Li, J. H. He and J. M. Lu, *J. Hazard. Mater.*, 2021, **409**, 125027.
4. R. Y. Xie, K. J. Fang, Y. Liu, W. C. Chen, J. N. Fan, X. W. Wang, Y. F. Ren and Y. W. Song, *J. Mater. Sci.*, 2020, **55**, 11919-11937.
5. H. Y. Liu, C. G. Niu, H. Guo, C. Liang, D. W. Huang, L. Zhang, Y. Y. Yang and L. Li, *J. Colloid Interface Sci.*, 2020, **576**, 264-279.
6. M. M. Sun, Z. Y. Chen and Y. Y. Bu, *Surf. Coat. Technol.*, 2015, **266**, 79-87.
7. G. Yang, D. M. Chen, H. Ding, J. J. Feng, J. Z. Zhang, Y. F. Zhu, S. Hamid and D. W. Bahnemann, *Appl. Catal. B*, 2017, **219**, 611-618.
8. Z. H. Chen, R. L. Liang, X. X. Guo, J. Y. Liang, Q. T. Deng, M. Li, T. X. An, T. C. Liu and Y. S. Wu, *Biosens. Bioelectron.*, 2017, **91**, 60-65.
9. X. Y. Meng, X. Chen, W. H. Wu, W. Zheng, H. H. Deng, L. Y. Xu, W. Chen, Z. L. Li and H. P. Peng, *Microchim. Acta*, 2019, **186**, 855.
10. L. Qu, L. Yang, Y. Y. Li, X. Ren, H. Wang, D. W. Fan, X. Y. Wang, Q. Wei and H. X. Ju, *ACS Appl. Mater. Interfaces*, 2021, **13**, 5795-5802.
11. Y. Zeng, J. Bao, Y. N. Zhao, D. Q. Huo, M. Chen, M. Yang, H. B. Fa and C. J. Hou, *Talanta*, 2018, **178**, 122-128.

12.S. Kumar, S. Panwar, S. Kumar, S. Augustine and B. D. Malhotra, *Nanomaterials*, 2019, **9**, 1190.

13.S. Kumar, J. Kumar and S. N. Sharma, *Mater. Res. Express*, 2018, **5**, 120338.

14.N. Pachauri, K. Dave, A. Dinda and P. R. Solanki, *J. Mater. Chem. B*, 2018, **6**, 3000-3012.

15.T. T. Wu, J. H. Feng, S. T. Zhang, L. Liu, X. Ren, D. W. Fan, X. Kuang, X. Sun, Q. Wei and H. X. Ju, *Biosens. Bioelectron.*, 2020, **169**, 112580.

16.Q. Q. Zhang, Y. M. Fu, K. Xiao, C. C. Du, X. H. Zhang and J. H. Chen, *Anal. Chem.*, 2021, **93**, 6801-6807.

17.Y. Y. Yu, Z. N. Huang, Y. Zhou, L. H. Zhang, A. L. Liu, W. Chen, J. H. Lin and H. P. Peng, *Biosens. Bioelectron.*, 2019, **126**, 1-6.